



CHORUS

This is the accepted manuscript made available via CHORUS. The article has been published as:

## Exact Coherent Structures and Phase Space Geometry of Preturbulent 2D Active Nematic Channel Flow

Caleb G. Wagner, Michael M. Norton, Jae Sung Park, and Piyush Grover

Phys. Rev. Lett. **128**, 028003 — Published 13 January 2022

DOI: [10.1103/PhysRevLett.128.028003](https://doi.org/10.1103/PhysRevLett.128.028003)

# Exact coherent structures and phase space geometry of pre-turbulent 2D active nematic channel flow

Caleb G. Wagner,<sup>1</sup> Michael M. Norton,<sup>2</sup> Jae Sung Park,<sup>1</sup> and Piyush Grover<sup>1</sup>

<sup>1</sup>*Mechanical and Materials Engineering, University of Nebraska - Lincoln, Lincoln, NE 68588*

<sup>2</sup>*School of Physics and Astronomy, Rochester Institute of Technology, Rochester, NY 14623*

Confined active nematics exhibit rich dynamical behavior, including spontaneous flows, periodic defect dynamics, and chaotic ‘active turbulence’. Here, we study these phenomena using the framework of Exact Coherent Structures, which has been successful in characterizing the routes to high Reynolds number turbulence of passive fluids. Exact Coherent Structures are stationary, periodic, quasiperiodic, or traveling wave solutions of the hydrodynamic equations that, together with their invariant manifolds, serve as an organizing template of the dynamics. We compute the dominant Exact Coherent Structures and connecting orbits in a pre-turbulent active nematic channel flow, which enables a fully nonlinear but highly reduced order description in terms of a directed graph. Using this reduced representation, we compute instantaneous perturbations that switch the system between disparate spatiotemporal states occupying distant regions of the infinite dimensional phase space. Our results lay the groundwork for a systematic means of understanding and controlling active nematic flows in the moderate to high activity regime.

Active matter is a class of materials composed of interacting and energy-consuming constituents. The past two decades have seen active matter grow into a new paradigm of nonequilibrium matter, with applications to both synthetic and biological systems [1]. Under the influence of particle-level driving forces, the emergent spatiotemporal structures of active matter are free to explore a much larger state space than available to passive equilibrium materials. Behaviors with no known equilibrium analogue include flocking and swarming [2–8], athermal clustering of spheres [9–13], spontaneous flows [14–22], and low Reynolds number ‘active’ turbulence [23–27].

There is an extensive theoretical framework for understanding and manipulating emergent structures in materials at or near equilibrium. However, there is not yet an equivalent framework for active matter. In this paper, we make progress towards this goal in the context of active nematics (AN), which are suspensions of active, rod-like, and apolar components [25, 28]; examples include bacterial films and cell colonies [29, 30]. Some of the most distinct phenomenology of AN occurs under confinement, in which case diverse spatiotemporal flow patterns are observed, including states of active turbulence [18, 25, 31–35]. There is much interest in learning to navigate this large space of spatiotemporal structures, for example steering a system toward a desired end state or switching between states [36–38]. In addition, there are fundamental unanswered questions related to active turbulence: how active fluids become turbulent, how to characterize them, and how to promote or inhibit transition to turbulence [27, 39].

Here we take a deterministic dynamical systems approach to these questions, beginning with the hydrodynamic equations governing AN. The dynamical systems approach has provided fresh insight into the long-standing problem of transition to turbulence in *passive*, *high Reynolds number* fluid flows [45]: the core premise,

going back to [46, 47], considers the fluid to be a deterministic dynamical system evolving in an infinite dimensional phase space [48]. The dominant flow patterns are understood in terms of *Exact Coherent Structures* (ECS) and the dynamical pathways connecting them. An ECS is a (generically unstable) stationary, periodic, quasiperiodic, or traveling wave solution of the hydrodynamic equations. Each ECS possesses invariant manifolds that are dynamical pathways connecting regions of phase space. A finite set of ECS, together with their invariant manifolds, constitutes a reduced-order but exact characterization of the global phase space. Though each ECS is non-turbulent, this representation is fully adequate for describing turbulent flows, which appear as chaotic trajectories meandering through the phase space and visiting the neighborhoods of different ECS in a recurring fashion [49–51]. Therefore, the ECS and their invariant manifolds act as an organizing template for the complicated spatiotemporal motion of the fluid. In inertial fluids, control strategies using this framework [52–54] are being explored for suppressing or delaying the transition to turbulence and reducing viscous dissipation. Recently, the approach has also been extended to elastoinertial [55] and viscoelastic [56] turbulence.

However, similar insight is missing in *active, low Reynolds number fluids*. Previous work on pre-turbulent flows has focused on discovering stable solutions and tracking equilibria through primary bifurcations [18, 34, 57, 58], while fully developed turbulence has been studied using coarse-grained statistical descriptions [27, 59–62] that do not deal primarily with deterministic dynamics.

In this work, we take a first step toward developing a dynamical systems picture of AN turbulence, focusing on the ECS and heteroclinic connections in a 2D channel in the pre-turbulent regime. We conducted a comprehensive search for the most dynamically relevant objects, which led to the discovery of three coexisting attractors—two

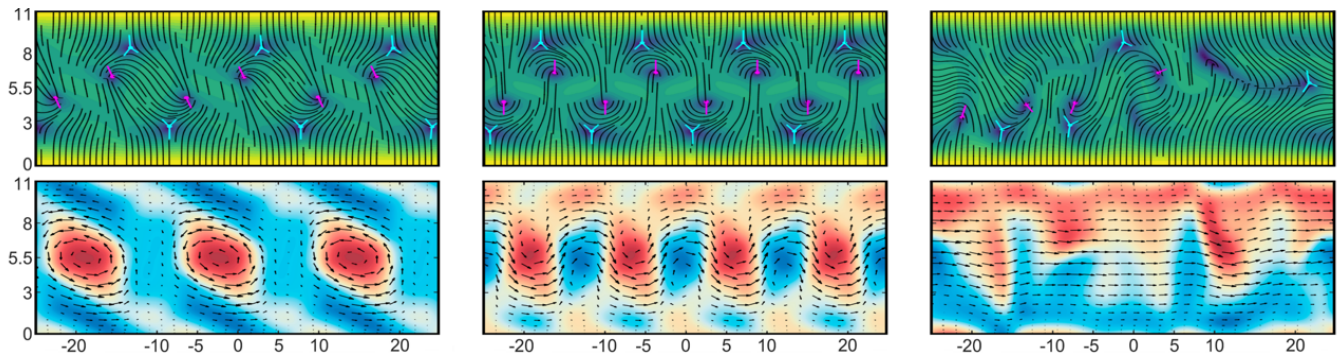


FIG. 1: Snapshots of three Exact Coherent Structures (ECS). The top plots show the nematic director field overlaid on the nematic order parameter (color gradient), and the bottom plots show the velocity field overlaid on the vorticity. **Left column:**  $\text{PO}_{3a}$ , a periodic orbit with a 3-fold translational symmetry. **Middle column:**  $\text{RPO}_{u4}$ , a relative periodic orbit that cycles between a vortex lattice (as shown) and a nearly unidirectional, defect-less flow. **Right column:**  $\text{RPO}_{1c}$ , a relative periodic orbit without obvious spatial structure. Movies S1-S5 show the dynamics of each ECS [44].

periodic orbits and a low-dimensional chaotic set—and 44 unstable ECS [44]. Away from the attractors, the phase space has complex global structure shaped by the unstable ECS and their invariant manifolds. In particular, the ECS dictate which of the three attractors a given flow configuration will evolve toward.

Our results go beyond previous work on AN in that they generate a reduced-order picture of the exact nonlinear dynamics: because the ECS framework is rooted in global relationships among exact time-dependent objects, it does not involve phenomenological approximations or restrictions to locally linear analysis. Moreover, our computation of *unstable* structures leads to new insight into the origin of stable structures and the dynamical paths leading to them. In particular, this understanding allows control of AN flows with minimal external input.

**Nematohydrodynamic Model.**—We model the AN in terms of the velocity  $\mathbf{u}(\mathbf{r}, t) = (u, v)$ , and nematic alignment tensor  $\mathbf{Q}(\mathbf{r}, t)$ . The latter is symmetric and traceless and can be parameterized as  $Q_{ij} = q(n_i n_j - 0.5\delta_{ij})$ , where the scalar  $q$  and unit vector  $\hat{\mathbf{n}}$  describe the degree and direction of nematic ordering. The domain is a periodic 2D channel, parameterized as  $(x, y) \in [-L/2, L/2] \times [0, h]$ , with  $x$  the periodic coordinate. The channel walls impose a no-slip boundary condition on  $\mathbf{u}$  and strong perpendicular anchoring on  $\mathbf{Q}$ . Following earlier work, we describe the dynamics using the hydrodynamic equations

$$\begin{aligned} \rho(\partial_t + \mathbf{u} \cdot \nabla) \mathbf{u} &= -\nabla p + \nabla \cdot (2\eta \mathbf{E} - \alpha \mathbf{Q}), \\ (\partial_t + \mathbf{u} \cdot \nabla) \mathbf{Q} + \mathbf{Q} \cdot \Omega - \Omega \cdot \mathbf{Q} &= \Gamma \mathbf{H}, \\ \nabla \cdot \mathbf{u} &= 0. \end{aligned} \quad (1)$$

The first and last lines are the incompressible Navier–Stokes equations, with  $p$  the pressure,  $\mathbf{E}$  and  $\Omega$  the strain rate and vorticity tensors, and  $\eta$  the viscosity. The term  $\nabla \cdot (\alpha \mathbf{Q})$  is the active dipolar density that drives the system. Recent work has shown that the resulting energy fluxes are dominated by viscous dissipation and inertial energy transfer [64]; hence, we omit terms describ-

ing passive elastic stresses. The dynamics of  $\mathbf{Q}$  consists of: (1) advective and rotational coupling to the velocity and the vorticity, and (2) relaxation via the molecular field  $\mathbf{H} = \mathcal{A} \mathbf{Q} - \mathcal{B} \mathbf{Q} \text{Tr}(\mathbf{Q}^2) + K \nabla^2 \mathbf{Q}$  toward configurations that minimize an effective free energy functional. Here  $\mathcal{A}$ ,  $\mathcal{B}$ , and  $\Gamma$  are material constants describing bulk properties of the nematic, and  $K$  is an elastic constant characterizing the energy cost of spatial variations in  $\mathbf{Q}$ . We focus on a single parameter set, working in units such that  $\rho = \eta = 1$ ,  $\mathcal{A} = 0.1$ ,  $\mathcal{B} = 0.5$ ,  $\Gamma = 0.34$ ,  $K = 0.04$ , and choose channel dimensions  $L = 50$  and  $h = 11$  in these units. We fix  $\alpha$  such that the non-dimensional activity  $A \equiv h\sqrt{\alpha/K}$  equals 15.5. For comparison, the nematic has an intrinsic length  $L_n = \sqrt{K/\mathcal{A}} \simeq 0.63$ , which is roughly the radius of a defect core, and activity induces the length scale  $L_a = \sqrt{K/\alpha} \simeq 0.71$ , which measures the balance between active and elastic stresses. We also observe that the velocity magnitude is roughly 0.01–0.1, which corresponds to Reynolds number  $\text{Re} \sim 0.1$ –1. Finally, we note that Ref. [34] and others incorporate additional terms in Eqs. 1 that account for *flow alignment*, which is the coupling between  $\mathbf{Q}$  and the symmetric part of the flow gradients. Here, we neglect these terms to focus on the essential aspects of the problem [65, 66].

To emphasize the phase space approach, we rewrite Eqs. 1 as  $\dot{X} = F(X)$ , where  $X = [\mathbf{u}, \mathbf{Q}]$  denotes the state of the system. The associated flow map is  $f^t(X_0) = X_0 + \int_0^t F(X(\tau)) d\tau$ , where  $X_0$  is the initial condition. Since ECS are generically unstable, they cannot be computed from direct time-dependent simulations; rather, one searches for solutions to certain fixed point equations (FPEs). The FPE for an equilibrium solution  $X_{\text{eq}}$  is just  $F(X_{\text{eq}}) = 0$ , while any point  $X_P$  on a periodic orbit (PO) satisfies  $f^T(X_P) = X_P$ , where  $T$  is the time period. Similarly, a point  $X_{\text{RP}}$  on a relative periodic orbit (RPO) satisfies  $f^T(X_{\text{RP}}) = \tau_x(\ell) X_{\text{RP}}$ , where  $\tau_x(\ell)$  is a streamwise translation by  $\ell$ . Hence, an RPO is a field profile that recurs at a streamwise-shifted location after time  $T$ . In

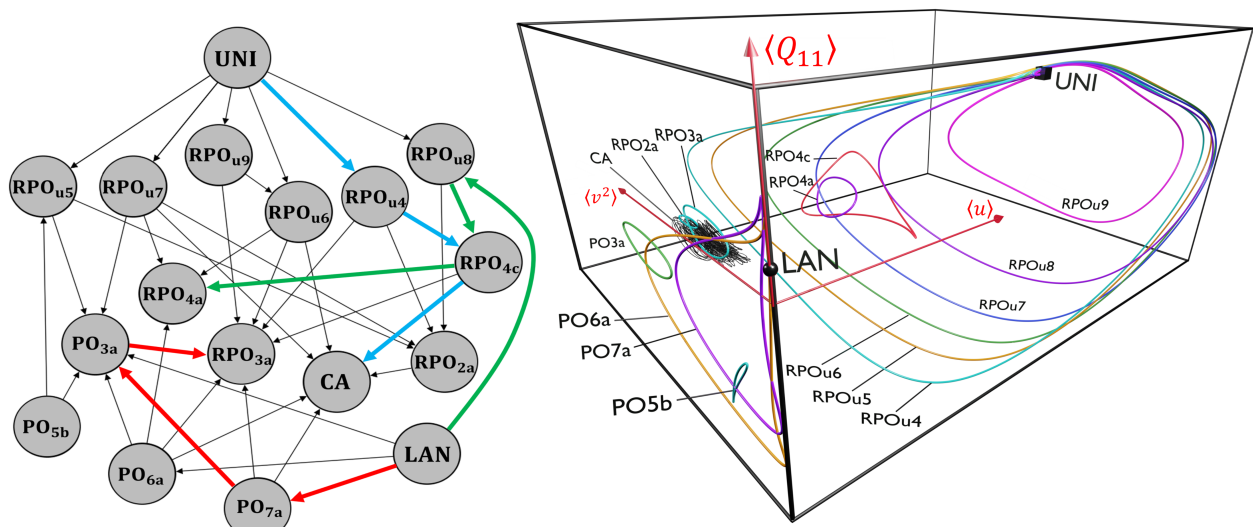


FIG. 2: **Left:** Directed graph representation of the phase space, with ECS (and the CA) as nodes and heteroclinic connections as edges. The colored arrows (red, green, blue) highlight three multistep connections that Fig. 3 visualizes in more detail. **Right:** ECS in a reduced 3D phase space  $(\langle u \rangle, \langle v^2 \rangle, \langle Q_{11} \rangle)$ , where  $\langle \cdot \rangle$  denotes the instantaneous channel average. The channel average removes the continuous translation symmetry [63], such that RPOs are closed orbits rather than tori in this representation. The laning equilibrium (LAN) and POs have no net streamwise flow and therefore lie on the  $\langle u \rangle = 0$  plane. The right drifting ( $\langle u \rangle > 0$ ) unidirectional equilibrium, RPOs, and chaotic attractor have left drifting counterparts ( $\langle u \rangle < 0$ ) (not shown). See movie S6 for a 360° view [44].

phase space, an RPO densely covers the surface of a two-torus. We also compute heteroclinic connections between pairs of ECS [67], which are trajectories that depart the ‘source’ ECS along its unstable manifold and converge to the ‘destination’ ECS along its stable manifold.

**Symmetries.**—Eqs. (1) are equivariant under the one-parameter group of  $x$  translations,  $\tau_x(\ell)$ , as well as the following  $x$  and  $y$  reflections, denoted  $\sigma_x$  and  $\sigma_y$ :

$$\begin{aligned}\sigma_x[u, v, Q_{11}, Q_{12}](x, y) &= [u, -v, Q_{11}, -Q_{12}](x, h - y), \\ \sigma_y[u, v, Q_{11}, Q_{12}](x, y) &= [-u, v, Q_{11}, -Q_{12}](L - x, y).\end{aligned}$$

If a state initially possesses any symmetries derived from these group operations, then it will retain the same symmetries under time evolution by Eqs. 1 [63]. Some ECS and heteroclinic connections fall into such invariant subspaces, while others possess no symmetries at all (Fig. 1). As our results below illustrate, these symmetries are powerful tools for analyzing the phase space geometry.

**Methods.**—Our computations use the open-source pseudospectral code Dedalus [68]. For channel geometries, Dedalus implements a Fourier basis for the periodic directions and Chebyshev polynomials for the wall-normal direction. All ECS and connections reported here were computed using 256 Fourier modes and 64 Chebyshev modes, corresponding to phase space dimension  $\approx 4 \times 256 \times 64 = 65536$ . To solve the FPEs, we use modified Newton-Raphson algorithms [69]. Two key ingredients are adaptive ‘hookstep’ step-size selection to improve global convergence [70], and a matrix-free GMRES [71, 72] algorithm for solving the linear BVP at each iteration. The matrix-free methods are essential because

they scale efficiently to the large problem dimensions encountered in hydrodynamic simulations. Finally, finding a new ECS requires a good initial guess for the FPE solver. Here, we devise initial guesses using a combination of (1) the global search method of [72] that samples arbitrary time-dependent trajectories for approximate solutions to the FPEs, (2) symmetry reduction [73], and (3) branch continuation in channel width; see the supplemental material [44] for details.

**Results.**—In time-dependent simulations, the dominant attracting state roughly passes through the following sequence of transitions as activity is increased: (1) zero-flow state; (2) defect-less, unidirectional flow; (3) vortex lattice with motile defects (‘dancing disclinations’); (4) spatiotemporal chaos (turbulence). These results generally agree with [34], which considers a similar AN model in channel confinement. The main difference is that the stable vortex lattice is an RPO in our case and a PO in [34]. This difference appears to arise from the effects of flow alignment, as we recover the results of [34] at sufficiently large values of flow alignment.

In this Letter, we discuss the phase space structure at an intermediate non-dimensional activity,  $A \equiv \sqrt{\frac{\alpha h^2}{K}} = 15.5$ , where the system has several co-existing attractors and saddle-type ECS. While this system is pre-turbulent, the phase space is quite rich, and there are numerous heteroclinic connections between ECS. Fig. 2 shows the dominant ECS in a reduced 3D phase space, alongside several connections as a directed graph. In addition to the unidirectional equilibria (UNI), we also found a pair of laning equilibria (LAN), in which

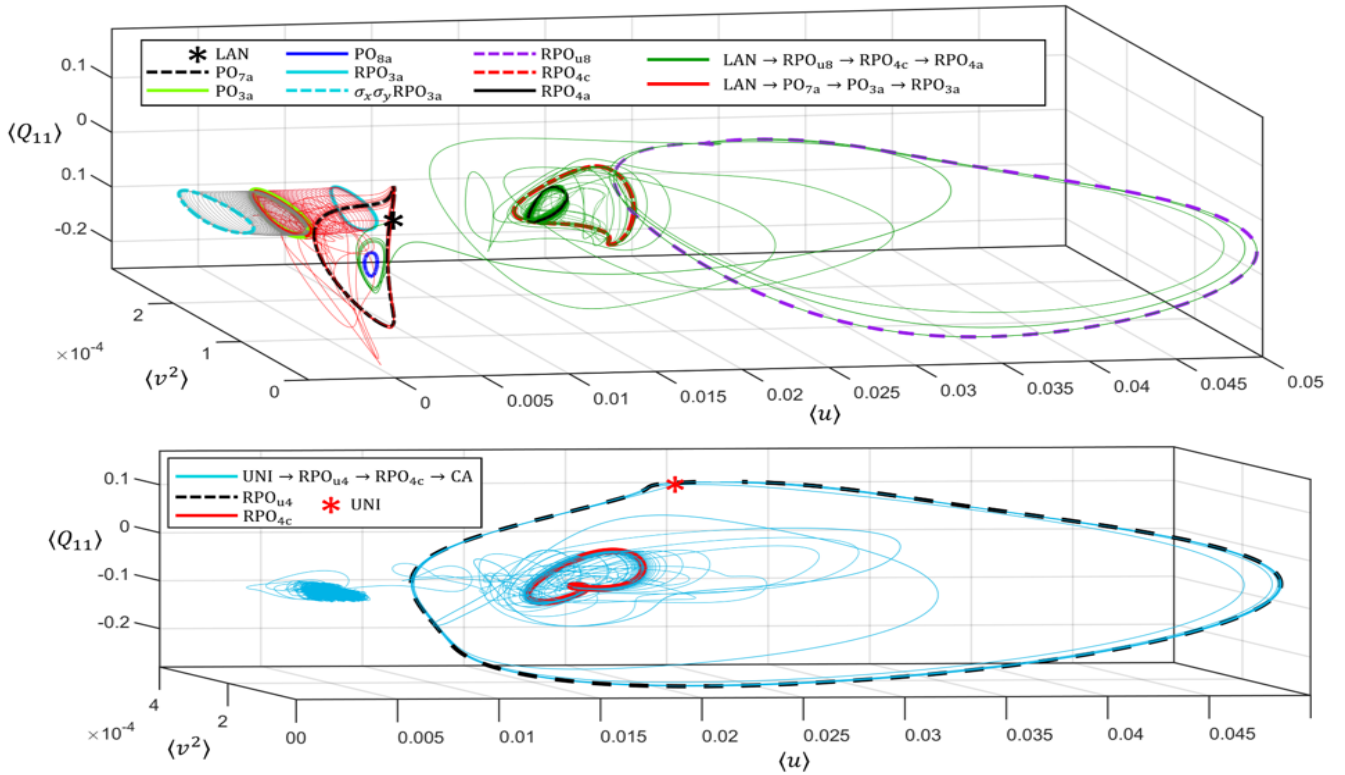


FIG. 3: Four connecting orbits in the reduced phase space obtained from the graph representation in Fig. 2. Such orbits can be constructed for a pair of ECS if a directed path exists between them in the graph. Each orbit is formed by patching together heteroclinic connections between successive ECS along the path using small perturbations. **Top:** Green shows the connection  $LAN \rightarrow RPO_{u8} \rightarrow RPO_{4c} \rightarrow RPO_{4a}$ . Red shows two connections: both starting with  $LAN \rightarrow PO_{7a} \rightarrow PO_{3a}$  and then perturbed toward either the left- or right-flowing version of  $RPO_{3a}$ . These last segments (red and gray) highlight the two-dimensional unstable manifold of  $PO_{3a}$ . **Bottom:** Blue shows the connection  $UNI \rightarrow RPO_{u4} \rightarrow RPO_{4c} \rightarrow CA$  (chaotic attractor). The dynamics of each connection are shown in movies S7-S9 [44].

the upper and lower halves of the channel flow in opposite directions,  $\pm u(y) = \mp u(h-y)$  and  $v=0$ . Both UNI and LAN are independent of  $x$ .

*Periodic Orbits.*—We found 11 unstable POs with  $k$ -vortex lattice structure for  $3 \leq k \leq 8$ , which we label  $PO_{k\zeta}$  for  $\zeta = a, b, \dots$ . Each  $PO_{k\zeta}$  has  $2k$  defect pairs and is invariant under the action of  $\mathbb{T}_k \equiv \tau_x(L/k)$  and  $\sigma_x \sigma_y$ . They are unstable versions of the previously reported stable ‘dancing disclinations’ solutions [34, 74].

*Relative Periodic Orbits.*—We found 33 RPOs, which we grouped based on their symmetries and relation to each other in phase space. One family, labeled  $RPO_{uk}$  for  $4 \leq k \leq 9$ , cycles between a  $k$ -fold vortex-like structure and a defect-free, nearly unidirectional flow. The time period of these RPOs diverges as activity is decreased from  $A = 15.5$ , which leads us to conjecture that they are born as homoclinic orbits to the unidirectional equilibrium (UNI). The remaining RPOs are grouped based on their (exact or approximate) discrete translational symmetry  $\mathbb{T}_k$ , and labeled as  $RPO_{k\zeta}$  for  $\zeta = a, b, \dots$ . Some are left and right drifting versions of the  $PO_{k\zeta}$  family; others appear more closely related to the  $RPO_{uk}$  family or lack distinct structure altogether. Under the action of

$\sigma_x \sigma_y$ , an RPO is transformed into its ‘opposite drifting’ counterpart, changing the sign on the shift  $\ell$ .

*Attractors.*—We found three attractors, not counting copies related by symmetry transformations. One is a chaotic attractor (CA), and hence, not an ECS. Rather, it is a higher-dimensional set localized to a cigar-shaped region of the 3D phase space projection, and containing trajectories that look like broken or frustrated versions of a 3-fold ‘dancing disclinations’ state. We confirmed the set is chaotic using the 0-1 test, which takes a time series as input and outputs a binary indicator for the presence of chaos; see [44]. The other two attractors are RPOs:  $RPO_{3a}$  and  $RPO_{4a}$ . They consist of 3 and 4-fold ‘rolling vortices’ and have the appearance of drifting versions of the dancing disclinations POs (see movie S3 in [44]). The reason that 3 and 4 are the only ‘allowed’ number of vortices in the attractors is that they accommodate the preferred active length scale intrinsic to the dynamics [75], whereas in wider channels, any RPO attractors have a proportionally larger number of vortices.

*Heteroclinic connections.*—Individual ECS lend structure to localized regions of phase space. To understand the *global* structure, we compute heteroclinic connec-

tions, which are special dynamical pathways connecting ECS. These reveal, for instance, the relationship between the  $RPO_{uk}$  family and the UNI equilibrium: by choosing a perturbation with  $k$ -fold translational symmetry, a trajectory starting on UNI passes directly onto  $RPO_{uk}$ . There are myriad other connections both inside and outside the ECS families. Some involve relatively little change in structure; for instance,  $PO_{3a}$  and  $PO_{4b}$  connect to their left and right flowing RPO counterparts. Others display striking changes in structure along non-trivial paths in phase space that, at first glance, seem unlikely to be found by our search strategy. For example, some trajectories starting from a  $k$ -fold PO have their  $k$ -fold symmetry destroyed before eventually landing on the *unstable*  $PO_{3a}$  and acquiring a 3-fold symmetry. In reality, these and similar connections are not accidental: in most cases they occur because the target ECS is stable in an invariant subspace.  $PO_{3a}$ , for example, is stable in the  $\sigma_x\sigma_y$  subspace. Nonetheless, there may be non-trivial connections that have little to do with invariant subspaces and require more systematic search tools, such as the nonlinear adjoint method [76]. See Tables S3-S12 for a list of ECS and heteroclinic connections [44].

**Directed graph representation.**—In experiments, one might wish to direct the system toward a specific attractor. In fact, our framework allows for more complex control objectives involving unstable ECS, which is a necessary prelude to engineering turbulent AN flows, where *all* ECS are unstable. The centerpiece of this control capability is a reduced-order representation of the phase space in terms of a *directed graph*, in which ECS and the CA are nodes, and heteroclinic connections are edges (Fig. 2). This representation uncovers nontrivial relationships in phase space, which can be exploited to induce desired transitions using minimal external control input. For instance, such methods have been used to discover low-energy dynamical channels forming an ‘interplanetary superhighway’ in the solar system [77]. Fig. 3 provides four examples of connecting orbits between distant ECS that were found by patching together heteroclinic connections using small perturbations.

**Conclusion.**—The characterization and control of far-from-equilibrium dynamics is a key step in realizing the promise of active matter. We have employed the Exact Coherent Structure approach to obtain a tractable, reduced-order representation of a model AN system. At higher activities, this approach can lead to a better understanding of transitional turbulence in active fluids. In experiments, the reduced-order representation can be exploited by applying external vorticity [78], light [36, 37], or pressure [58] modulation to reach and maintain otherwise inaccessible spatiotemporal states.

**Acknowledgements.**—We thank Aparna Baskaran, Predrag Cvitanović, Seth Fraden, Mike Hagan and Ashley Willis for helpful discussions. This material is based upon work supported by the U.S. Department of Energy,

Office of Science, Office of Basic Energy Sciences under award number DE-SC0022280.

- 
- [1] G. Gompper, R. G. Winkler, T. Speck, A. Solon, C. Nardini, F. Peruani, H. Lwen, R. Golestanian, U. B. Kaupp, L. Alvarez, T. Kiorboe, E. Lauga, W. C. K. Poon, A. DeSimone, S. Muiños-Landin, A. Fischer, N. A. Sker, F. Cichos, R. Kapral, P. Gaspard, M. Ripoll, F. Sagues, A. Doostmohammadi, J. M. Yeomans, I. S. Aranson, C. Bechinger, H. Stark, C. K. Hemelrijk, F. J. Nedelec, T. Sarkar, T. Aryaksama, M. Lacroix, G. Duclos, V. Yashunsky, P. Silberzan, M. Arroyo, and S. Kale, *J. Phys. Condens. Matter* **32**, 193001 (2020).
  - [2] J. Toner and Y. Tu, *Phys. Rev. Lett.* **75**, 4326 (1995).
  - [3] J. Toner, Y. Tu, and S. Ramaswamy, *Annals of Physics* **318**, 170 (2005).
  - [4] T. Vicsek and A. Zafeiris, *Phys. Rep.* **517**, 71 (2012).
  - [5] A. Attanasi, A. Cavagna, L. D. Castello, I. Giardina, T. S. Grigera, A. Jelić, S. Melillo, L. Parisi, O. Pohl, E. Shen, and M. Viale, *Nat. Phys.* **10**, 691 (2014).
  - [6] A. Attanasi, A. Cavagna, L. Del Castello, I. Giardina, S. Melillo, L. Parisi, O. Pohl, B. Rossaro, E. Shen, E. Silvestri, and M. Viale, *PLoS Comput. Biol.* **10**, e1003697 (2014).
  - [7] A. Cavagna, D. Conti, C. Creato, L. D. Castello, I. Giardina, T. S. Grigera, S. Melillo, L. Parisi, and M. Viale, *Nature Physics* **13**, 914 (2017).
  - [8] K. van der Vaart, M. Sinhuber, A. M. Reynolds, and N. T. Ouellette, *Sci. Adv.* **5**, eaaw9305 (2019).
  - [9] Y. Fily and M. C. Marchetti, *Phys. Rev. Lett.* **108**, 235702 (2012).
  - [10] G. S. Redner, M. F. Hagan, and A. Baskaran, *Phys. Rev. Lett.* **110** (2013).
  - [11] J. Stenhammar, A. Tiribocchi, R. J. Allen, D. Marenduzzo, and M. E. Cates, *Phys. Rev. Lett.* **111**, 145702 (2013).
  - [12] I. Buttinoni, J. Bialké, F. Kümmel, H. Löwen, C. Bechinger, and T. Speck, *Phys. Rev. Lett.* **110**, 238301 (2013).
  - [13] M. E. Cates and J. Tailleur, *Annu. Rev. Condens. Matter Phys.* **6**, 219 (2015).
  - [14] M. B. Wan, C. J. Olson Reichhardt, Z. Nussinov, and C. Reichhardt, *Phys. Rev. Lett.* **101**, 018102 (2008).
  - [15] J. Tailleur and M. E. Cates, *EPL (Europhysics Letters)* **86**, 60002 (2009).
  - [16] L. Angelani, C. Maggi, M. L. Bernardini, A. Rizzo, and R. Di Leonardo, *Phys. Rev. Lett.* **107**, 138302 (2011).
  - [17] P. K. Ghosh, V. R. Misko, F. Marchesoni, and F. Nori, *Phys. Rev. Lett.* **110**, 268301 (2013).
  - [18] L. Giomi, L. Mahadevan, B. Chakraborty, and M. Hagan, *Nonlinearity* **25**, 2245 (2012).
  - [19] D. Marenduzzo, E. Orlandini, and J. M. Yeomans, *Phys. Rev. Lett.* **98** (2007).
  - [20] L. Giomi, M. C. Marchetti, and T. B. Liverpool, *Phys. Rev. Lett.* **101** (2008).
  - [21] A. Bricard, J.-B. Caussin, N. Desreumaux, O. Dauchot, and D. Bartolo, *Nature* **503**, 95 (2013).
  - [22] Y. Baek, A. P. Solon, X. Xu, N. Nikola, and Y. Kafri, *Phys. Rev. Lett.* **120**, 058002 (2018).
  - [23] C. Dombrowski, L. Cisneros, S. Chatkaew, R. E. Gold-

- stein, and J. O. Kessler, Phys. Rev. Lett. **93**, 098103 (2004).
- [24] H. H. Wensink, J. Dunkel, S. Heidenreich, K. Drescher, R. E. Goldstein, H. Lowen, and J. M. Yeomans, PNAS **109**, 14308 (2012).
- [25] A. Doostmohammadi, J. Ignés-Mullol, J. M. Yeomans, and F. Sagués, Nat. Commun. **9**, 1 (2018).
- [26] C. Blanch-Mercader, V. Yashunsky, S. Garcia, G. Duclos, L. Giomi, and P. Silberzan, Phys. Rev. Lett. **120** (2018).
- [27] R. Alert, J. Casademunt, and J.-F. Joanny, arXiv preprint arXiv:2104.02122 (2021).
- [28] M. C. Marchetti, J.-F. Joanny, S. Ramaswamy, T. B. Liverpool, J. Prost, M. Rao, and R. A. Simha, Rev. Mod. Phys., **85**, 1143 (2013).
- [29] Y. I. Yaman, E. Demir, R. Vetter, and A. Kocabas, Nat. Commun. **10** (2019).
- [30] D. Dell’Arciprete, M. L. Blow, A. T. Brown, F. D. C. Farrell, J. S. Lintuvuori, A. F. McVey, D. Marenduzzo, and W. C. K. Poon, Nat. Commun. **9** (2018).
- [31] F. C. Keber, E. Loiseau, T. Sanchez, S. J. DeCamp, L. Giomi, M. J. Bowick, M. C. Marchetti, Z. Dogic, and A. R. Bausch, Science **345**, 1135 (2014).
- [32] A. Opathalage, M. M. Norton, M. P. Juniper, B. Langeslay, S. A. Aghvami, S. Fraden, and Z. Dogic, PNAS **116**, 4788 (2019).
- [33] K.-T. Wu, J. B. Hishamunda, D. T. Chen, S. J. DeCamp, Y.-W. Chang, A. Fernández-Nieves, S. Fraden, and Z. Dogic, Science **355**, eaal1979 (2017).
- [34] T. N. Shendruk, A. Doostmohammadi, K. Thijssen, and J. M. Yeomans, Soft Matter **13**, 3853 (2017).
- [35] G. Duclos, R. Adkins, D. Banerjee, M. S. Peterson, M. Varghese, I. Kolvin, A. Baskaran, R. A. Pelcovits, T. R. Powers, A. Baskaran, F. Toschi, M. F. Hagan, S. J. Streichan, V. Vitelli, D. A. Beller, and Z. Dogic, Science **367**, 1120 (2020).
- [36] T. D. Ross, H. J. Lee, Z. Qu, R. A. Banks, R. Phillips, and M. Thomson, Nature **572**, 224 (2019).
- [37] R. Zhang, S. A. Redford, P. V. Ruijgrok, N. Kumar, A. Mozaffari, S. Zemsky, A. R. Dinner, V. Vitelli, Z. Bryant, M. L. Gardel, and J. J. de Pablo, arXiv preprint arXiv:1912.01630 (2019).
- [38] M. M. Norton, P. Grover, M. F. Hagan, and S. Fraden, Phys. Rev. Lett. **125**, 178005 (2020).
- [39] M. J. Bowick, N. Fakhri, M. C. Marchetti, and S. Ramaswamy, arXiv preprint arXiv:2107.00724 (2021).
- [40] G. Yalnız, B. Hof, and N. B. Budanur, Phys. Rev. Lett. **126**, 244502 (2021).
- [41] F. Verhulst, *Nonlinear differential equations and dynamical systems* (Springer Science & Business Media, 2006).
- [42] G. A. Gottwald and I. Melbourne, Proc. R. Soc. A **460**, 603 (2004).
- [43] G. A. Gottwald and I. Melbourne, “The 0-1 test for chaos: A review,” in *Chaos Detection and Predictability*, edited by C. H. Skokos, G. A. Gottwald, and J. Laskar (Springer Berlin Heidelberg, Berlin, Heidelberg, 2016) pp. 221–247.
- [44] See Supplemental Material [url], which includes Refs. [40–43, 67, 69].
- [45] M. D. Graham and D. Floryan, Annu. Rev. Fluid Mech. **53** (2020).
- [46] E. Hopf, Commun. Pure Appl. Math. **1**, 303 (1948).
- [47] D. Ruelle and F. Takens, Les rencontres physiciens-mathématiciens de Strasbourg-RCP25 **12**, 1 (1971).
- [48] P. Cvitanović, J. Fluid. Mech. **726**, 1 (2013).
- [49] J. S. Park and M. D. Graham, J. Fluid. Mech. **782**, 430 (2015).
- [50] N. B. Budanur, A. S. Dogra, and B. Hof, Phys. Rev. Fluids **4**, 102401 (2019).
- [51] B. Suri, L. Kageorge, R. O. Grigoriev, and M. F. Schatz, Phys. Rev. Lett. **125**, 064501 (2020).
- [52] E. A. Davis and J. S. Park, J. Fluid. Mech. **894** (2020).
- [53] M. Linkmann, F. Knierim, S. Zammert, and B. Eckhardt, J. Fluid. Mech. **900** (2020).
- [54] D. Lucas, arXiv preprint arXiv:2008.08388 (2020).
- [55] Y. Dubief, J. Page, R. R. Kerswell, V. E. Terrapon, and V. Steinberg, arXiv preprint arXiv:2006.06770 (2020).
- [56] J. Page, Y. Dubief, and R. R. Kerswell, Phys. Rev. Lett. **125**, 154501 (2020).
- [57] M. M. Norton, A. Baskaran, A. Opathalage, B. Langeslay, S. Fraden, A. Baskaran, and M. F. Hagan, Phys. Rev. E **97**, 012702 (2018).
- [58] J. Walton, G. McKay, M. Grinfeld, and N. J. Mottram, Eur. Phys. J. E **43**, 1 (2020).
- [59] H. H. Wensink, J. Dunkel, S. Heidenreich, K. Drescher, R. E. Goldstein, H. Löwen, and J. M. Yeomans, PNAS **109**, 14308 (2012).
- [60] M. Linkmann, G. Boffetta, M. C. Marchetti, and B. Eckhardt, Phys. Rev. Lett. **122**, 214503 (2019).
- [61] M. Linkmann, M. C. Marchetti, G. Boffetta, and B. Eckhardt, Phys. Rev. E **101**, 022609 (2020).
- [62] S. Mukherjee, R. K. Singh, M. James, and S. S. Ray, arXiv preprint arXiv:2105.07872 (2021).
- [63] P. Cvitanovic, R. Artuso, R. Mainieri, G. Tanner, G. Vattay, N. Whelan, and A. Wirzba, ChaosBook.org (Niels Bohr Institute, Copenhagen 2005) **69**, 25 (2005).
- [64] C.-M. Koch and M. Wilczek, arXiv preprint arXiv:2107.14167 (2021).
- [65] S. Shankar, S. Ramaswamy, M. C. Marchetti, and M. J. Bowick, Phys. Rev. Lett. **121**, 108002 (2018).
- [66] M. L. Blow, M. Aqil, B. Liebchen, and D. Marenduzzo, Soft matter **13**, 6137 (2017).
- [67] B. Suri, R. K. Pallantla, M. F. Schatz, and R. O. Grigoriev, Phys. Rev. E **100**, 013112 (2019).
- [68] K. J. Burns, G. M. Vasil, J. S. Oishi, D. Lecoanet, and B. P. Brown, Phys. Rev. Res. **2**, 023068 (2020).
- [69] D. Viswanath, J. Fluid. Mech. **580**, 339 (2007).
- [70] J. E. Dennis and R. B. Schnabel, *Numerical Methods for Unconstrained Optimization and Nonlinear Equations* (SIAM, 1996).
- [71] Y. Saad and M. H. Schultz, SIAM J. Sci. Comput. **7**, 856 (1986).
- [72] G. J. Chandler and R. R. Kerswell, J. Fluid. Mech. **722**, 554 (2013).
- [73] A. P. Willis, P. Cvitanović, and M. Avila, J. Fluid. Mech. **721**, 514 (2013).
- [74] A. J. Tan, E. Roberts, S. A. Smith, U. A. Olvera, J. Arteaga, S. Fortini, K. A. Mitchell, and L. S. Hirst, Nature Physics **15**, 1033 (2019).
- [75] L. Giomi, Phys. Rev. X **5**, 031003 (2015).
- [76] M. Farano, S. Cherubini, J.-C. Robinet, P. De Palma, and T. Schneider, J. Fluid. Mech. **858** (2019).
- [77] W. S. Koon, M. W. Lo, J. E. Marsden, and S. D. Ross, Chaos **10**, 427 (2000).
- [78] D. P. Rivas, T. N. Shendruk, R. R. Henry, D. H. Reich, and R. L. Leheny, Soft Matter **16**, 9331 (2020).